Eur. Phys. J. B **14**, 639–648 (2000)

THE EUROPEAN PHYSICAL JOURNAL B

EDP Sciences

Structure and properties of some glass-forming liquid alloys

U. Dahlborg[1,a], M. Calvo-Dahlborg[1,b], P.S. Popel[2], and V.E. Sidorov[2]

[1] Department of Neutron Physics, Royal Institute of Technology, 10044 Stockholm, Sweden
[2] Ural State Pedagogical Institute, Cosmanavtov Ave. 26, 620119, Ekaterinburg, Russia

Received 25 February 1999 and Received in final form 28 October 1999

Abstract. Some physical properties (kinematic viscosity, surface tension and magnetic susceptibility) of some Fe-based metallic melts of easily glass-forming alloys have been measured during heating and subsequent cooling. The results indicate that molten liquid metallic alloys undergo a number of structural transformations ranging from the initial microheterogeneous state formed after melting up to the true solution state. Studies by small angle neutron scattering on a eutectic SnPb melt confirm this conclusion in that two families of different sizes have been seen, one in the range 1 to 2 nm and one of size larger than 100 nm. Both kind of particles have relatively sharp interfaces and the size of the smaller particles is found to depend on temperature.

PACS. 61.12.Ex Neutron scattering techniques (including small-angle scattering) – 61.25.Mv Liquid metals and alloys

1 Introduction

The most efficient method for production of amorphous alloys is a rapid quench from the liquid state. However, it has been found that the temperature of the initial melt significantly affects the structure and properties of the produced amorphous ribbons. In order to understand the underlying physical phenomena, the influence of heat treatment of the molten alloy before quench has recently been investigated in several works [1–5]. The effects observed in measurements on several macroscopic physical properties of the melt, like viscosity, resistivity, etc., were explained either by free volume freezing or by deactivation of crystallisation centres when the alloy was heated far above the liquidus temperature [1,2]. However, the behaviour of some other physical properties can not be explained by the occurrence of any of these two processes, which indicates that other physical phenomena are involved. As an example, anomalous variations can be observed in "property *vs.* temperature" curves for some metal- metalloid alloys, such as Fe-B [4], Co-B [6], Ni-B [4], Fe-Co-B [3] and Ni-P [7] systems, but also in ternary alloys as Al-Ni-Ce and Al-Ni-La [8].

The possibility of structural changes occurring in metallic melts was indicated in some theoretical model calculations [9–13]. It was shown in [14] that after the melting of the heterogeneous initial alloy, a microheterogeneous melt is formed. One can consider it as a metastable non-equilibrium microemulsion or as a microsuspension of disperse particles enriched in one of the components and surrounded by a molten matrix of different composition. These particles are thus inherited from the initial material. They seem to have sharp but irregular interfaces [4,15–17] and a more or less homogeneous internal structure and local properties. One can therefore identify them as a disperse phase of the colloidal melt. When heating the melt to a temperature, which is characteristic for its composition, the thermodynamic equilibrium between the particles and the melt matrix is destroyed and the system irreversibly transforms into a true solution state which is thermodynamically stable at all the above-liquidus temperatures. This transformation may be sharp but can also take place *via* several steps in the dispersion of the particles to smaller ones even in simple binary systems [4]. If the melt consists of three components or more, a set of disperse particles with various composition can exist in the microheterogeneous melt and each kind of particles start to dissolve at specific temperatures.

The paper presents some further experimental results on the heating-cooling effects in Fe-based liquid alloys susceptible to amorphisation. Some results on the composition dependence of these effects are also presented. In order to get a more direct evidence of the existence of "particles" of different sizes in metallic melts results from small angle neutron scattering measurements on a eutectic melt of SnPb are also reported. This system was chosen for several reasons, one being that the appropriate temperature range is easily accessible in a standard furnace. However, the non-corrosive behaviour of molten SnPb at

[a] now at Laboratoire de Science et Génie des Matériaux Métalliques, CNRS UMR 7584, École des Mines, 54042 Nancy Cedex, France
[b] e-mail: dahlborg@mines.u-nancy.fr

relatively high temperatures was also of great importance. Usually all alloys possible to rapidly quench to the amorphous state have a composition close to eutectic. Therefore SnPb can, because of its simple eutectic phase diagram, be regarded as a model system from which general conclusions on the microstructure of metallic melts may be drawn.

2 Experimental procedures

During the course of these investigations several experimental techniques yielding information on both atomic and mesoscopic scales have been used. Thus electron diffraction measurements in the general diffraction mode were carried out in order to determine the atomic structure of thin films of liquid Sn-Pb. The thickness of the films was of the order of 20–25 nm. Some investigations of the structure of bulk Sn-Pb were performed at the SLAD diffractometer at the Studsvik reactor, Sweden. Moreover, the microstructure (on the nanometer scale) was determined by small angle neutron scattering (SANS) measurements on the PACE diffractometer at the Orphée reactor, Laboratoire Léon Brillouin, Saclay, France. The covered wavevector transfer range was 0.07 to 2 nm^{-1} which corresponds to a range of about 1 to 80 nm in real space.

The density, ρ, of the molten alloys was measured by the γ-ray absorption method with an experimental error of 0.01% to 0.03% while the kinematic viscosity, ν, was determined by the damping decrement of the crucible torsion vibrations. The accidental error in the viscosity measurement did not exceed 1%. The magnetic susceptibility, χ, was measured by the Faraday method using a high sensitivity automatic balance with an experimental error of about 0.8%. The surface tension, σ, of the melts was obtained by the sessile drop method on the surface of a beryllium oxide plate in vacuum. The experimental error in this case amounts to about 1.5%.

3 Results

3.1 Fe-based melts

The temperature dependence of the kinematic viscosity, ν, of molten $Fe_{85}B_{15}$ obtained during heating of the alloy after melting and during the subsequent cooling is presented in Figure 1a. Three specific features of the measured curves should be noted: 1) The curves obtained during heating and cooling do not coincide, *i.e.* there is a hysteresis effect in the temperature variation of the viscosity. 2) The two curves join at high temperatures. 3) There is an anomalous behaviour of the heating curve at about 1 300 ℃ which is about 100 degrees above the liquidus for this composition. This temperature corresponds to the dissolution temperature, denoted T_d in the discussion below. It should be mentioned that the eutectic composition corresponds to $Fe_{83}B_{17}$ with the eutectic temperature 1 174 ℃. The two effects mentioned above seem to be

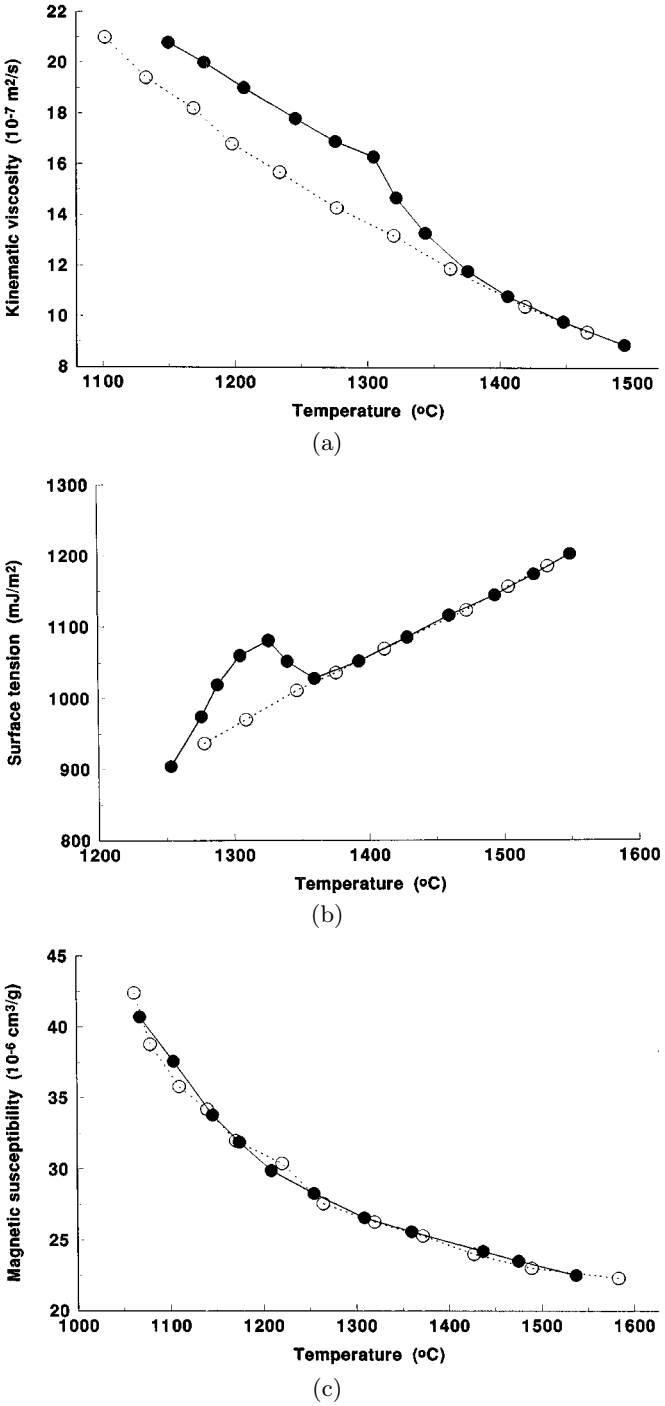

Fig. 1. The temperature dependence of (a) kinematic viscosity ν, (b) the surface tension σ, and (c) the magnetic susceptibility χ for $Fe_{85}B_{15}$ obtained during heating (•) and subsequent cooling (○).

reversible as after solidification and remelting the same effects are observed and the same values are measured within the experimental accuracy. The two curves meet above 1 450 ℃ at a temperature which below is denoted the branching temperature, T_b. As seen in Figure 1b, the surface tension exhibits on heating an anomaly at

about the same temperature as the viscosity. In addition, this quantity has a positive temperature coefficient during both heating and cooling which is in contradiction to what is common for one-component metallic melts. The temperature dependence of the magnetic susceptibility, presented in Figure 1c, does not exhibit any particular feature and the curves measured on cooling and heating coincide within the experimental error.

The temperature variation of the kinematic viscosity for the $Fe_{85-x}Co_xB_{15}$ melt of different compositions is shown in Figure 2. In no case, except for $x = 64$, there is an agreement between the cooling and heating curves. At most compositions the cooling curves are more or less continuous while the values obtained during heating have a very irregular temperature variation. However, the special features seen for the binary $Fe_{85}B_{15}$ alloy in Figure 1a are preserved when some of the Fe atoms are replaced by Co atoms. Fe and Co atoms can not be considered as substitutional in the melt as there are clear differences between Figures 2b and 2e and between Figure 1a and Figures 2a to 2f. Furthermore, the heating curve at equiatomic Fe and Co fraction exhibits the most irregular behaviour (*cf.* Fig. 2d). Another confirmation is given by the fact that the viscosity is decreasing monotonously with increasing Co content. An interesting feature seen in Figures 2a to 2f is that the anomaly in the heating curve becomes more and more pronounced and that T_d is gradually shifted to higher temperatures when the Co content increases up to 42 at%. For $x > 42$ this tendency is resumed. Accordingly, as the values on heating and cooling shown in Figure 2e agree, it may be conjectured that the alloy with a relative Fe:Co composition of 1:3 corresponds to a thermodynamically stable situation. It can thus be supposed that T_d is shifted to considerably higher temperatures for this composition. Moreover, it can also be mentioned that from the variation of the failure stress with relative Fe:Co composition in FeCoB metallic glasses produced by melt-spinning, clusters of stoichiometric compositions of 3:1, 1:1 and 1:3 have been suggested to exist in the ribbons [1,18].

The alloys possible to amorphise, are complicated eutectic systems, *i.e.* one or both phases of the solid eutectic consist of compounds. Some additional anomalous features can be seen in the temperature variation of several physical properties in many of these systems. To exemplify this, the temperature variation of the density in the Fe-B system containing 26.4 and 33.3 at% B is shown in Figure 3. The heating and cooling curves at 2:1 composition coincide, which shows that in this case no microheterogeneous liquid is formed after melting and that molten Fe_2B is homogeneous. However, this is not the case for an approximate 3:1 composition. A pronounced anomaly can be observed for both compositions close to 1 650 °C. This indicates that some reversible transformation involving only the short range order occurs both in homogeneous ($Fe_{66.7}B_{33.3}$) and in microheterogeneous ($Fe_{73.6}B_{26.4}$) alloys at this temperature which is considerably higher than the T_b found in $Fe_{85}B_{15}$. It is worth noticing in this connection that the melting points of Fe_2B and Fe_3B are both in the temperature region 1 340 to 1 400 °C.

3.2 Sn-Pb melt

3.2.1 Density measurements

The discrepancy in the temperature variation of the properties at heating and subsequent cooling, indicates that some irreversible changes of the structure of the melt take place at a temperature close to the branching point. To clarify the nature of these changes, a series of experiments was carried out on the model eutectic alloy $Sn_{73.9}Pb_{26.1}$. The sample was melted in a γ-ray densitometer furnace at about 800 °C, *i.e.* at a temperature considerably exceeding the eutectic point, $T_e = 183$ °C. After relaxation the density-temperature dependence was determined on cooling. Despite the high sensitivity of this method no peculiarities were registered for the density curve, $\rho(T)$, for temperatures down to T_e. The situation completely changes after crystallisation of the sample and its remelting (Fig. 4). On reheating the alloy, irregularities can be observed in the temperature variation of the density and a dissolution and branching temperatures, T_d and T_b, respectively, of similar kind as exemplified in Figures 1 and 2, can be defined as indicated by the arrow (T_d). At temperatures higher than the branching point the measured values of the density agree with the ones obtained on the first cooling and as well as with those measured during subsequent thermal cycling of the melt [14]. From Figure 4 it can be conjectured that T_d is at about 400 °C and T_b above 750 °C.

3.2.2 Diffraction measurements

It can from the results above be concluded that irreversible structural changes occur also in the eutectic PbSn melt during the primary heating after the melting of the initial sample. The nature of these structural changes was investigated by electron and neutron diffraction experiments. In the electron diffraction experiment it was observed that after melting of the sample, the shape of the atomic radial distribution function (RDF), as obtained by Fourier transformation of the structure factor (shown in Fig. 5), indicates the existence of the same interatomic distances as have been found in neutron diffraction measurements on liquid lead [20] and tin [21]. This confirms the presence of microheterogeneities in the melt, *i.e.* that the melt consists of small domains enriched in one of the components. This conclusion can also be arrived at from the comparison of the relative intensities of the main peak in $S(Q)$ (Fig. 5) and of the shoulder on its high Q side, taking into account the relative scattering powers of Sn and Pb and their concentration in the melt. Moreover, according to the results of sedimentation experiments [22,23] the characteristic size of the microdomains is of the order of 1 to 10 nm which substantially exceeds the short-range

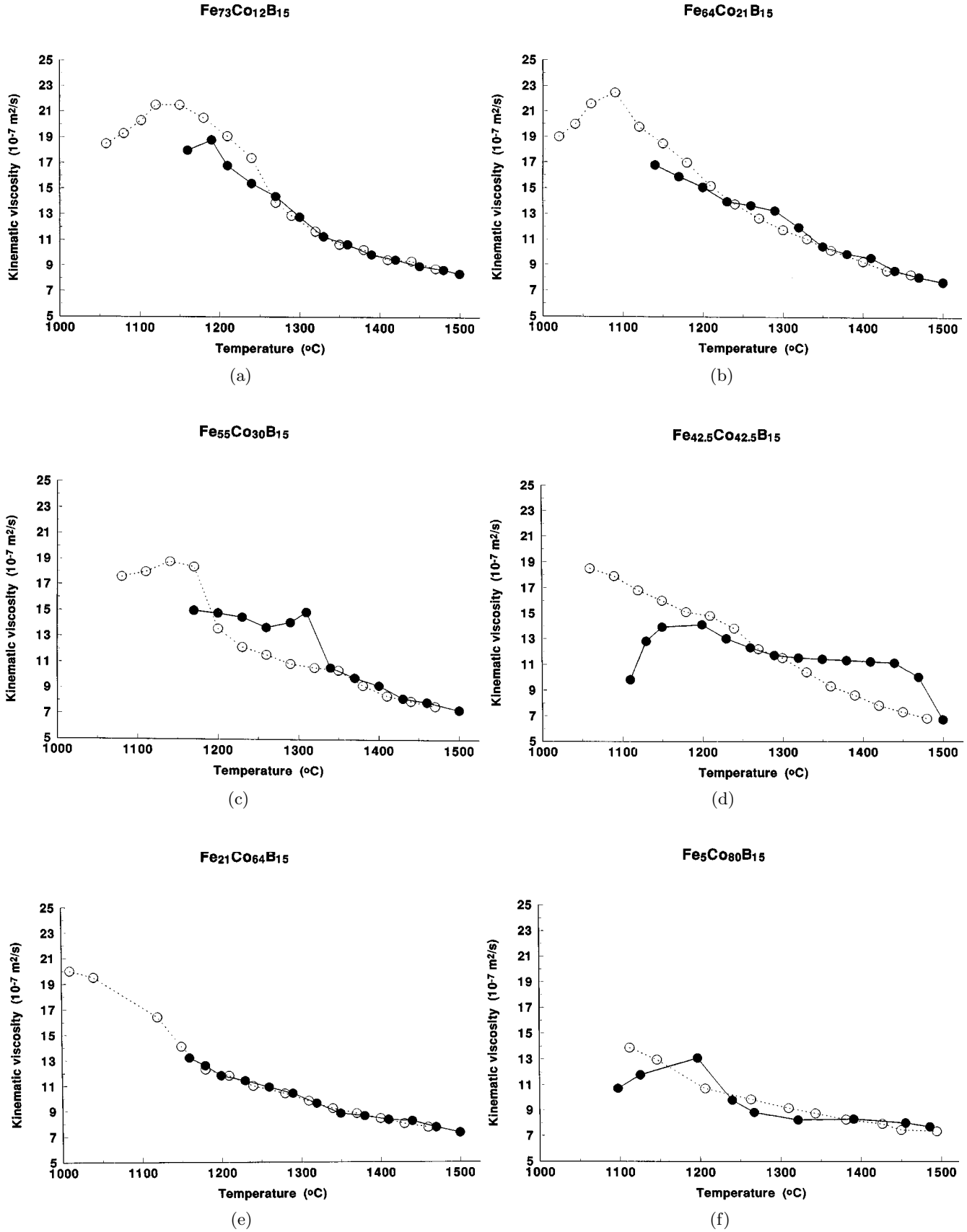

Fig. 2. Temperature dependence of the kinematic viscosity, ν, for $Fe_{85-x}Co_xB_{15}$ melts of different composition obtained during heating (•) and subsequent cooling (○). (a) $x = 12$; (b) $x = 21$; (c) $x = 30$; (d) $x = 42.5$; (e) $x = 64$; (f) $x = 80$.

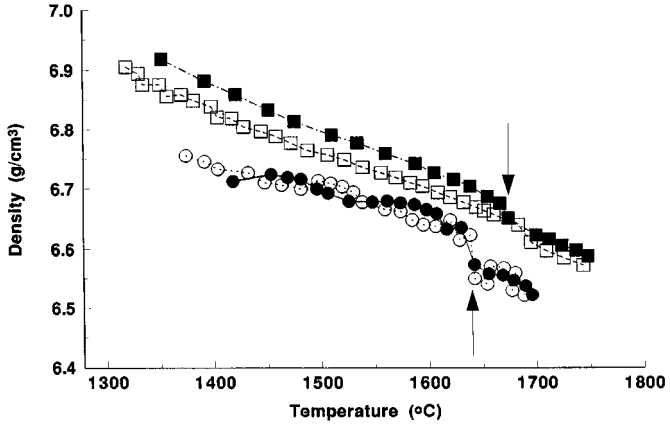

Fig. 3. Temperature dependence of the density, ρ, of $Fe_{73.6}B_{26.4}$ (squares) and $Fe_{66.7}B_{33.3}$ (circles) melts during heating after melting (filled symbols) and subsequent cooling (open symbols). The arrows show in each system the anomaly linked to the structural transformation of the liquid.

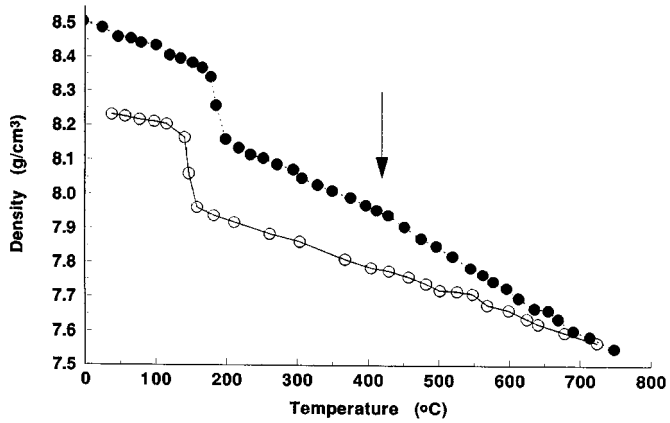

Fig. 4. Temperature dependence of density, ρ, of $Sn_{73.9}Pb_{26.1}$ melt ((•) heating after sample melting and solidification, (○) cooling after component mixing at 700 °C). The arrow indicates the temperature T_d.

order scale. During *in situ* heating in the electron microscope the structure changes shape. Above about 500 °C, which is above the temperature T_d of the anomaly in the $\rho(T)$ curve. This indicates that the microdomains either completely break up or disintegrate into smaller ones [14]. However, the melt becomes a true solution, a completely mixed liquid state, only above the branching temperature T_b.

The results obtained by electron diffraction are confirmed by real-time neutron diffraction investigations during a temperature loop on heating from room temperature up to 650 °C and subsequent cooling. The scattering cross section measured at 250 °C on heating is compared to the one measured at 650 °C in Figure 6a. The 250 °C curve has a shape similar to the curve obtained by electron diffraction with a distinct shoulder on the large Q side of the main peak (*cf.* Fig. 5). The curve measured at 650 °C is much smoother and no shoulder is seen which indicates that the structure has become more homogeneous. Figure 6b presents the difference between the structure factor measured on heating at 250 °C and the one measured at the same temperature on cooling after that the melt has been kept at 650 °C during 6 hours. The difference clearly

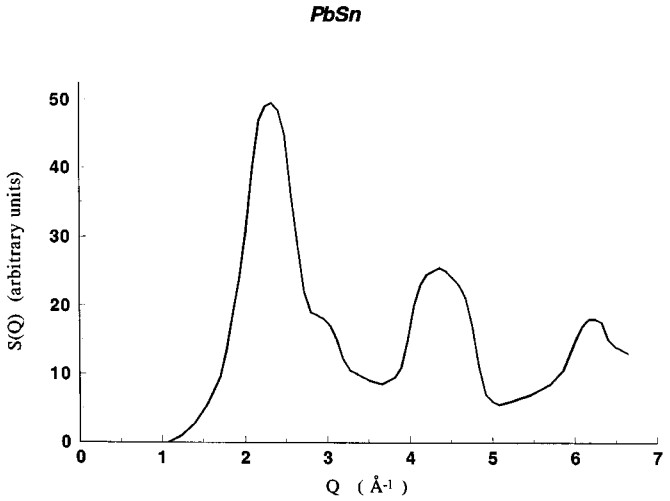

Fig. 5. Structure factor of a $Sn_{73.9}Pb_{26.1}$ liquid film measured by electron diffraction just above the eutectic temperature.

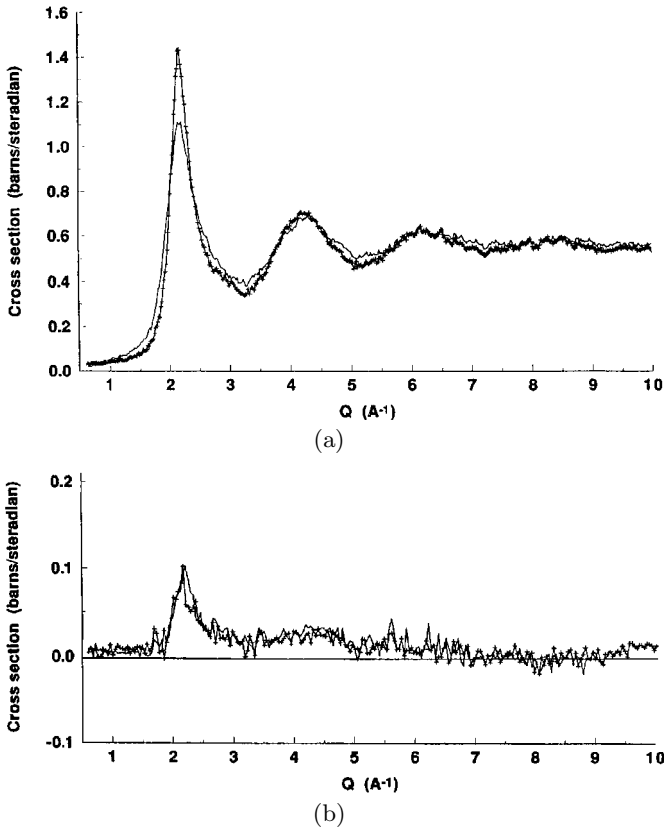

Fig. 6. (a) Structure factors of liquid $Sn_{74}Pb_{26}$ measured by neutron diffraction at 250 °C (broken line) and at 650 °C. (b) Difference between structure factors measured at 250 °C on heating and on cooling after heat treatment of the melt at 650 °C during 6 hours. The two curves correspond to different data sets.

shows that a homogenisation of the melt has occurred during this heat treatment and it confirms the hypothesis of dissolution of the microheterogeneities above T_d. It might be argued that 250 ℃ is below the melting points of pure Pb and Sn (327 ℃ and 232 ℃, respectively). A similar, however somewhat smaller difference, was observed from measurements at 350 ℃.

It should also be noted that 650 ℃ is below the temperature T_b. The observed difference would probably have been even larger if the heat treatment had been carried out up to a temperature above T_b, *i.e.* up to the domain where the liquid really has reached a true solution state. Moreover, when the sample in the liquid state was heated to a temperature below 500 ℃, it crystallised to the eutectic structure after cooling. However, after heating to about 800 ℃ the structure of an abnormally over-saturated solid solution of Pb in Sn, was observed in the electron diffraction pattern after crystallisation. This again confirms that at T_d the melt starts to transform and reaches the state of true solution at T_b and that at temperatures $T > T_b$ the thermodynamically stable state of a eutectic melt is the stable true solution. This also confirms that 650 ℃ was a too low temperature for observing clear effects. The microheterogeneity observed in the sample after melting below T_d is thus due to prolonged preservation of microsegregations in the liquid phase which are inherited from the heterogeneous eutectic ingot. In this connection it should again be emphasized that both T_d and T_b are considerably higher than the melting points of both lead and tin.

3.2.3 Small angle neutron scattering (SANS)

Brief theoretical background

The macroscopic differential cross section (MDCS) which determines the scattered intensity can generally for the case of a dilute and isotropically scattering system, consisting of non-interacting, randomly oriented particles, be written as [24]

$$\frac{\mathrm{d}\sigma}{\mathrm{d}\Omega}(Q) = \sum_j \sum_i (\rho_{ij} - \rho_\mathrm{m})^2 \times \int N_{ij}(s_i) V_i(s_i)^2 \left|F_i(Q, s_i)\right|^2 \mathrm{d}s_i \quad (1)$$

where index j represents particles with a given chemical composition. Q is the scattering vector. $F(Q, s_i)$ is the form factor of a scattering object of the topological type i. The topological type of an object is defined by its shape and the size s_i is a specific function of its dimensions (*e.g.* of the two axes in the case of an ellipsoid). $N_{ij}(s_i)$ represents the size distribution function of particles j of type i and $V_i(s_i)$ is the volume of the object of type i and size s_i. ρ_{ij} is the scattering length density (the sum of neutron scattering lengths per unit volume) of particle j and topological type i and ρ_m is that of the surrounding medium. The summation in equation (1) runs over all different kinds of particles of different type and size in the scattering system. The quantity $(\rho_{ij} - \rho_\mathrm{m})^2$ is called the contrast. Thus, according to equation (1), in a SANS experiment the strength of the measured signal is proportional to the contrast and not to the scattering length of individual nuclei, as is the case in an ordinary diffraction experiment.

The MDCS has some useful general properties which makes it possible to estimate the properties of the scattering system. For a two-phase system consisting of identical particles equation (1) can be simplified to [25]

$$\frac{\mathrm{d}\sigma}{\mathrm{d}\Omega}(Q) = \frac{V_\mathrm{p}^2 N_\mathrm{p}}{N} (\rho_\mathrm{p} - \rho_\mathrm{m})^2 \left|F_\mathrm{p}(Q)\right|^2 \quad (2)$$

where V_p is the particle volume and N_p the number of particles. It has been shown by Guinier that at small values of the product Qa, where a is a linear dimension of a particle, the quantity $\left|F_\mathrm{p}(Q)\right|^2$ can be approximated by $\left|F_\mathrm{p}(Q)\right|^2 = \exp(-Q^2 R_\mathrm{G}^2/3)$ for any particle shape [24]. R_G is denoted the radius of gyration and for a spherical particle of radius R it is given by $R_\mathrm{G} = (3/5)^{1/2} R$. The Guinier approximation is generally considered to be satisfactory for $QR_\mathrm{G} < 1$.

For $Qa > 1$, where a is the smallest dimension of the scattering particle, the Porod approximation can be used to extract information from a measured SANS curve [26]. For homogeneous particles with sharp boundaries this can be expressed as

$$\frac{\mathrm{d}\sigma}{\mathrm{d}\Omega}(Q) = \frac{K_\mathrm{p}}{Q^4} = \frac{2\pi(\rho_\mathrm{p} - \rho_\mathrm{m})^2 S}{V_\mathrm{T} Q^4} \quad (3)$$

where K_p is the Porod constant which is proportional to the total surface area S of the particles in a sample of volume V_T. It is also possible to obtain some information about the total volume fraction C_p of the precipitates by noting that the integral over the cross section, the so-called invariant, is related to C_p *via* [25]

$$\int Q^2 \frac{\mathrm{d}\sigma}{\mathrm{d}\Omega}(Q) \mathrm{d}Q = 2\pi^2 C_\mathrm{p}(1 - C_\mathrm{p})(\rho_\mathrm{p} - \rho_\mathrm{m})^2. \quad (4)$$

Experimental results

The SANS experiment was performed on a 10 mm thick sample of $Sn_{73.9}Pb_{26.1}$. Measurements were performed at five temperatures in one cycle, in a heating mode 250, 350 and 650 ℃ and during cooling at 350 and 250 ℃. The measured intensities $I(Q)$ of scattered neutrons, fully corrected for all instrumental effects, are presented in Figure 7 as a function of the neutron wavevector transfer Q ($Q \approx 2\pi\theta/\lambda$, where θ is the scattering angle and λ the wavelength of the incident neutrons). The signal is at all temperatures quite strong and it extends over the entire measured Q range. This unambiguously shows that the sample contains "particles" and that they have a very wide size distribution. By "particles" is meant regions in the liquid having a different composition than the environment. It should be emphasized that a sample, which is homogeneous on the length scale of the SANS experiment (in our case from about 0.5 to about 100 nm) and does

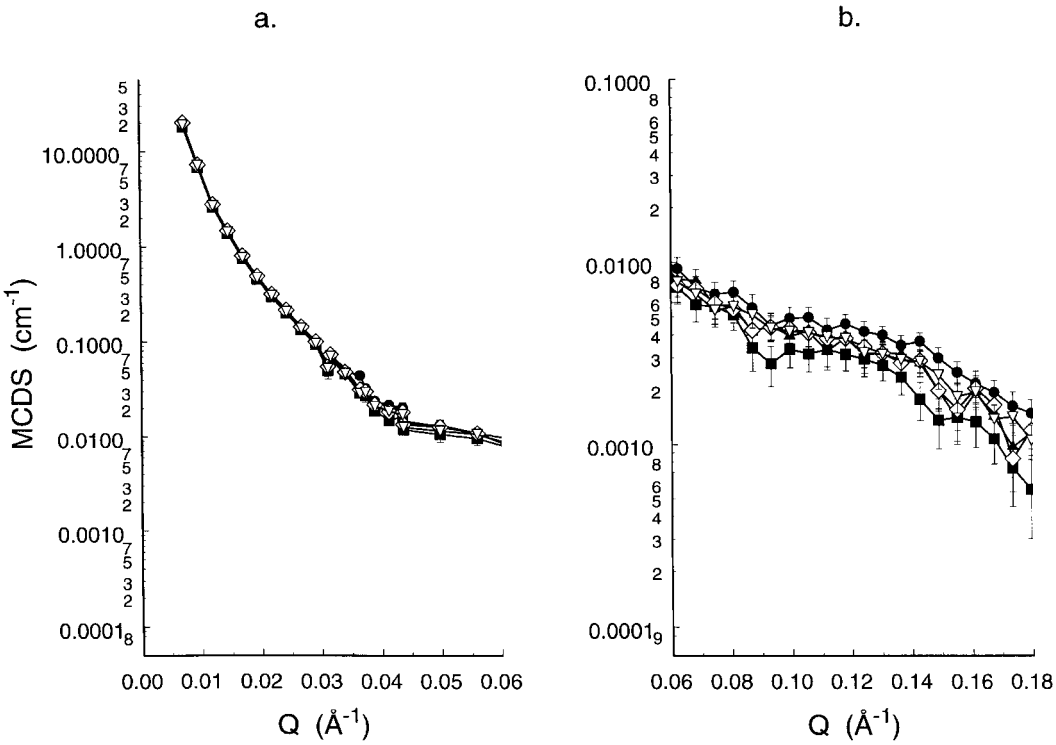

Fig. 7. The small angle neutron scattering intensity $I(Q)$, fully corrected, in the small (a) and large (b) wavevector transfer regions for $Sn_{73.9}Pb_{26.1}$ melt during one heating and subsequent cooling cycle. Heating: (•) 250 °C, (▲) 350 °C, (■) 650 °C. Cooling: (◇) 350 °C, (▽) 250 °C.

not contain interfaces of larger objects, does not give a small angle scattering signal [24].

The curves in Figure 7 have quite different behaviour in the low (Fig. 7a) and in the large (Fig. 7b) Q regions which indicates that there are at least two different kinds of particles with different size distribution present in the PbSn melt. This is even more obvious from Figures 8 and 9 which show the Q dependence of the quantities $Q^2I(Q)$ and $Q^4S(Q)$, respectively. As the intensity in the two Q regions seems to be clearly separated from each other, it is assumed for the further analysis that the total intensity can be described by a sum of two independent contributions, below denoted "particle set (1)" (corresponding to the small Q region) and "particle set (2)" (corresponding to the large Q region). In order to obtain both a qualitative and quantitative information on the nature of the two particle families, the low and the large Q regions were both fitted by the Guinier and the Porod expressions (Eqs. (2, 3) above). In order to check whether the data were fulfilling the Porod approximation, the power of Q in equation (3) was considered as a fitting parameter. In order to minimize any influence of one Q region on the other one, the fits were restricted to $0.007 < Q < 0.03$ and $0.13 < Q < 0.18$ Å^{-1}, respectively. It turned out that the only Q region where it was possible to get a satisfactory fit of the Guinier expression was $0.07 < Q < 0.11$ Å^{-1}. This range is compatible with the obtained value on R_G and with the region of validity of the Guinier approximation relative to the Porod approximation for particle set (2). The invariants were also calculated according to equation (4). For particle set (1) it was not possible to obtain a reliable value on the invariant. In order to include the contributions for particle set (2) from Q regions outside the ones covered in the measurements, the integrand was, for $0 < Q < 0.04$ Å^{-1}, approximated by a parabola. For $Q > 0.18$ Å^{-1} the Porod approximation (Eq. (3)) with the parameters from the fits were used. The obtained values from these fits, as well as the residual per measured Q, are compiled in Tables 1 and 2. The value at $Q = 0$ obtained from the Guinier fit is also included for comparative reasons only. The absolute values are, however, not considered to be accurate enough to render any basis for conclusions. The following conclusions can be drawn from Figures 7 to 9 and from Tables 1 and 2:

- The measured MDCSs coincide within statistical errors for small Q while in the large Q region they are affected by the heat treatment of the melt. When increasing the temperature from 250 to 650 °C, the intensity is monotonically decreasing while in the following cooling cycle the intensity at 350 and 250 °C are the same within the experimental errors, being the same as the intensity measured at 350 °C during heating.
- In the small Q region the fit of equation (3) yields a power of Q equal to 4.04 at all temperatures. Although this value is outside the computational error, the difference from the true Porod exponent is too small to be considered relevant and it will not be discussed below.

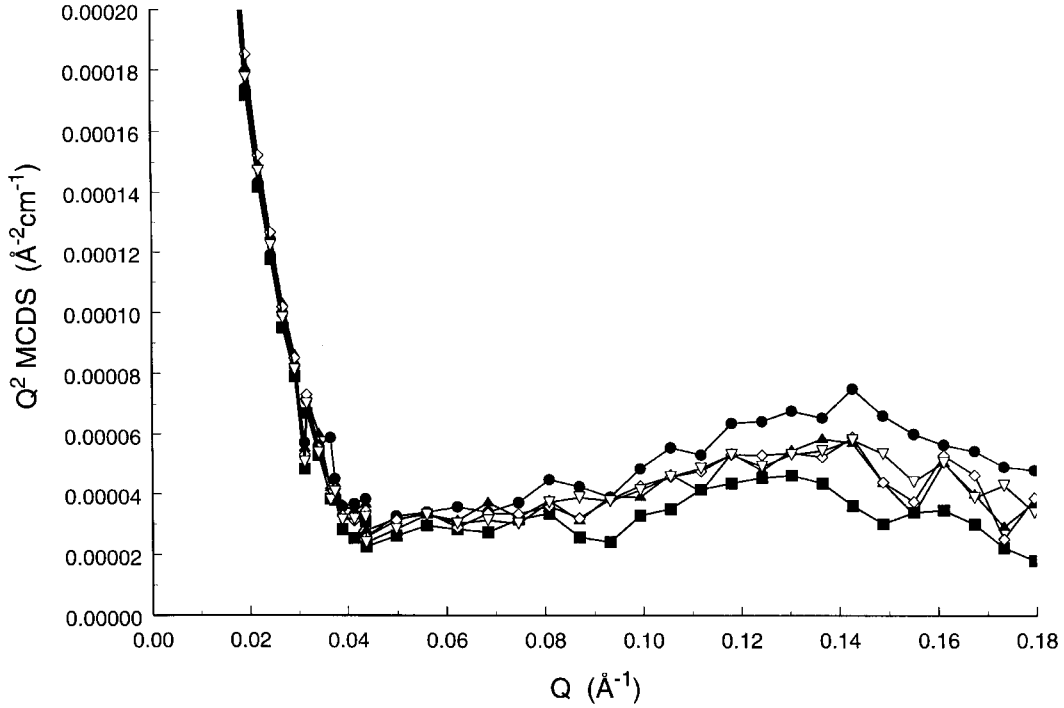

Fig. 8. The quantity $Q^2I(Q)$ for the $Sn_{73.9}Pb_{26.1}$ melt during one heating and subsequent cooling cycle. Heating: (•) 250 °C, (▲) 350 °C, (■) 650 °C. Cooling: (◇) 350 °C, (▽) 250 °C.

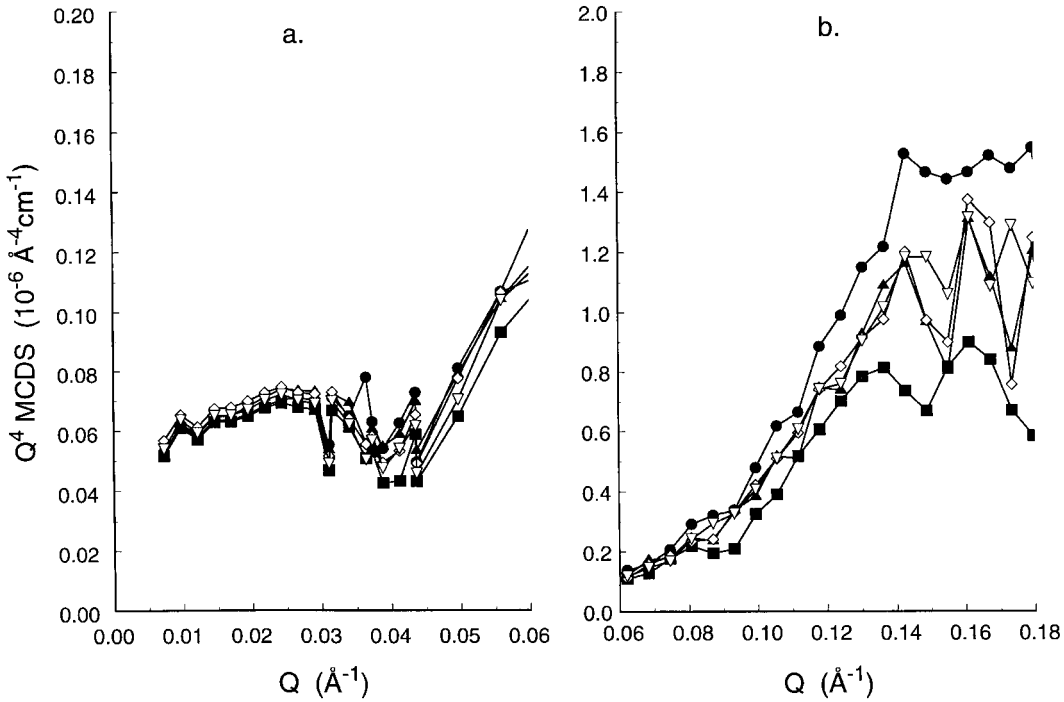

Fig. 9. The quantity $Q^4I(Q)$ for the $Sn_{73.9}Pb_{26.1}$ melt during one heating and subsequent cooling cycle in the small (a) and large (b) wavevector transfer regions. Heating: (•) 250 °C, (▲) 350 °C, (■) 650 °C. Cooling: (◇) 350 °C, (▽) 250 °C.

The values of the Porod constant are slightly decreasing with increasing temperature. As the density of the melt is changing with temperature (see Fig. 4) this decrease indicates that, even if the differences are within the estimated experimental errors, particle set (2) is unaffected by the heat treatment. The difference in measured intensities is entirely in accordance with the difference in contrast.

Table 1. Obtained values from fits of equation (3) to $I(Q)$ for in different Q regions. H denotes heating and C cooling modes, respectively.

Measurement		Porod fit for $0.03 < Q < 0.045$ Å^{-1}			Porod fit for $0.13 < Q < 0.18$ Å^{-1}		
Temp.	Mode	$10^8 K_P$	Exponent	$(10^3/n)\Sigma\delta^2$	$10^8 K_P$	Exponent	$(10^5/n)\Sigma\delta^2$
250 °C	H	7.2 ± 0.8	4.04 ± 0.01	6.4	151 ± 20	4.08 ± 0.01	4.3
350 °C	H	7.0 ± 0.8	4.04 ± 0.01	5.4	104 ± 14	4.09 ± 0.02	4.4
650 °C	H	6.5 ± 0.8	4.04 ± 0.00	7.9	76 ± 10	4.09 ± 0.02	1.8
350 °C	C	7.1 ± 0.8	4.04 ± 0.01	6.5	100 ± 15	4.09 ± 0.02	6.2
250 °C	C	6.9 ± 0.7	4.04 ± 0.00	6.7	107 ± 18	4.09 ± 0.02	3.7

Table 2. Obtained values from fits of $I(Q) = I(0)\exp(-R_G^2 Q^2/3)$ to the experimental data in the region $0.07 < Q < 0.11$ Å^{-1} and the invariant calculated as mentioned in the text. H denotes heating and C cooling modes, respectively.

Measurement		Guinier fit			Invariant
Temp.	Mode	$I(0) \times 10^3$	R_G^2 (Å^2)	$(10^5/n)\Sigma\delta^2$	(10^{-7} Å^{-4} cm^{-1})
250 °C	H	5.4 ± 0.4	73 ± 15	4.0	6.4 ± 0.8
350 °C	H	4.4 ± 0.3	63 ± 15	4.1	5.3 ± 0.7
650 °C	H	3.9 ± 0.5	54 ± 19	7.1	4.3 ± 0.6
350 °C	C	4.3 ± 0.2	52 ± 14	1.8	5.3 ± 0.7
250 °C	C	4.4 ± 0.2	53 ± 16	1.5	5.3 ± 0.7

- In the large Q region the Porod exponent is found to be in the range 4.08–4.09 independent of temperature and the difference from 4 is here considered to be significant. An exponent greater than 4 has been explained by the existence of a fuzzy particle boundary [27].
- As the radius of gyration R_G obtained from a Guinier fit is independent of the contrast, the values shown in Table 2 indicate that the particle set (2) is irreversibly changing size during the heat treatment. Assuming that the particles have spherical shape the average particle radius is decreasing from about 11 Å at 250 °C to about 9 Å at 650 °C. The cooling from 650 °C does not affect the particle size. The values of the Porod constant and of the invariant are also found to decrease during the heating cycle and remain constant during the subsequent cooling. This decrease is substantially larger than the one which can be accounted for by the density (contrast) variation and it shows that the number of particles is decreasing during heating and that no recombination is taking place during the subsequent cooling. The temperature variation of all these three quantities, as well of the intensity at $Q = 0$, $I(0)$, obtained by the Guinier fit, given in Table 2 is entirely consistent.

4 Discussion

From the results presented above it can be concluded that the anomaly at T_d and the branching at T_b of the heating and cooling curves are caused by an irreversible change of the microheterogeneity scale in the system. These changes, which ultimately lead to the true solution state at T_b, depend on the chemical composition of the alloy, on the difference in valence between the constituent atoms as well as on the chemical species which exist in the specific composition range according to the phase diagram. The irreversible transition of the melt to the true solution state sometimes proceeds through several stages. For example, evidence of such a sequence of transitions was observed during investigation of the temperature dependence of the density in Ni-B alloys [4]. Furthermore, the preservation of the positive sign of the surface tension temperature coefficient (*cf.* Fig. 1b) confirms that the overheating of the Fe-based alloys was not taking place at a sufficiently high temperature to provide full destruction of the microheterogeneities because the system did not fully transform into the state of the true solution in the covered temperature range. Anomalies in the temperature dependencies of the viscosity and the surface tension coefficients during heating of $Fe_{85}B_{15}$ around 1 300 °C (*cf.* Figs. 1a and 1b) are related to a structural change of the microheterogeneous melt. This is probably not connected to large rearrangements on an interatomic scale as no distinct anomaly can be observed in the temperature variation of the magnetic susceptibility which is rather sensitive to modifications of the short-range order of a system. However, it has been found that the temperature derivative of the susceptibility exhibits a small anomaly at about 1 400 °C [3].

The microheterogeneities, found in amorphous materials produced by melt quenching and discussed in many works [1–3,5,15,16,28], can thus be explained by the existence of different melt microheterogeneous states before quench. As emphasized in [5] it can thus be concluded that the microheterogeneities, found to exist in metallic

glasses, are partly inherited from the original melts being in a metastable or non-equilibrium microheterogeneous state at the time of the quench. This greatly influences the physical properties of the produced alloys. This hypothesis has also been confirmed by numerous results on various Fe- and Ni-based alloys [1–3,5,15,16,28] as well as on $Al_{91}La_5Ni_4$ and $Al_{91}Ce_5Ni_4$ alloys [8]. During the investigation of the viscosity in the liquid state, a hysteresis, similar to the ones shown in Figures 1 and 2, was observed in all cases. Thus, in order to study the influence of the thermodynamic state of the melt on the properties of rapidly solidified ribbons, several series of ribbons were prepared after various overheating schemes of the melt before the quench. First investigations of the mechanical behaviour of ribbons solidified from temperatures below T_b, show that they are more brittle and in some cases can even be considered as partly crystalline [28,29]. It was furthermore found that ribbons prepared from higher melt temperatures, were more ductile and amorphous. A detailed description of these results will be published elsewhere.

5 Conclusion

The results presented in this study confirm that molten liquid metallic alloys undergo during heating a number of structural transformations ranging from the initial microheterogeneous state formed after melting or component mixing up to the true solution state. Two temperatures can thus be defined: i) T_d, the dissolution temperature which corresponds to the anomaly in the heating curves and to the start of the dissolution of the microheterogeneities and ii) T_b, the branching temperature which corresponds to the development of a true solution state.

The authors are grateful for the financial support from the Swedish Institute which made part of this work possible. M.C-D. and U.D. also acknowledge the assistance of D. Lairez, R. Bellissent and V. Thevenot during the measurements on PACE at the Orphée reactor, Laboratoire Léon Brillouin, Saclay, France.

References

1. V.P. Manov, S.I. Popel, P.I. Buler, Rasplavy (Melts) **1**, 23 (1989) (in Russian).
2. V.P. Manov, S.I. Popel, P.I. Buler, A.B. Manukhin, D.G. Komlev, Mat. Sci. Eng. A **133**, 535 (1991).
3. V.E. Sidorov, M. Calvo-Dahlborg, U. Dahlborg, P.S. Popel, S. Chernoborodova, J. Mat. Sci. (in press).
4. P.S. Popel, V.E. Sidorov, Mat. Sci. Eng. A **226/228**, 237 (1997).
5. M. Calvo-Dahlborg, Mat. Sci. Eng. A **226/228**, 833 (1997).
6. E.V. Kolutukhin, V.S. Cepelev, P.S. Popel, Rasplavy **2**, 25 (1988).
7. V.E. Sidorov, Doctor Thesis, Ural State Pedagogical Institute, Ekaterinburg, Russia, 1998.
8. V.P. Manov, A. Rubshtein, A. Voronel, P.S. Popel, A. Vereshagin, Mat. Sci. Eng. A **179/180**, 535 (1994).
9. A.C. Mitus, A.Z. Patashinki, Physica A **150**, 383 (1988).
10. J.A. Knapp, D.M. Follsteadt, Phys. Rev. Lett. **58**, 2454 (1987).
11. R. Goswani, K. Chattopadhyay, Mat. Sci. Eng. A **179/180**, 163 (1994).
12. V.M. Barboi, Y.M. Glasman, G.I. Fuks, Coloidnyo Zhurnal USSR **32**, 233 (1970).
13. P.S. Popel, B. Baum, Metally **5**, 47 (1986) (in Russian).
14. P.S. Popel, O.A. Chikova, V.M. Matveev, High Temp. Mat. Proc. **4**, 219 (1995).
15. U. Dahlborg, M. Calvo-Dahlborg, R.K. Heenan, J.M. Ruppert, V.E. Sidorov, P.S. Popel (preprint).
16. U. Dahlborg, M. Calvo-Dahlborg, in *Proceeding International Workshop on "Mechanical Properties of Metallic Glasses", Ústav experimentálnej fyziky SAV, Kosiče, Slovakia, 22–24 September 1998*, p. 17.
17. U. Dahlborg, M. Calvo-Dahlborg (preprint).
18. E.D. Tabachnikova, V.Z. Bengus, P. Duhaj, G. Vlasak, V.P. Popov, T.A. Lobkovskaya, Mat. Sci. Eng. A **226-228**, 361 (1997).
19. V.Z. Bengus, P. Duhaj, in *Proceeding International Workshop on "Mechanical Properties of Metallic Glasses", Ústav experimentálnej fyziky SAV, Kosiče, Slovakia, 22–24 September 1998*, p. 1.
20. U. Dahlborg, M. Davidovic, K.E. Larsson, Phys. Chem. Liq. **6**, 149 (1977).
21. D.M. North, J.E. Enderby, P.A. Egelstaff, J. Phys. C **1**, 1075 (1968).
22. A.A. Vartman, A.M. Samarin, A.M. Yakobson, Technical Sciences Branch, Metallurgy and Fuel **3**, 1331 (1960).
23. R. Kumar, C.S. Sivaramakrishnan, J. Mater. Sci. **4**, 377 (1969).
24. A. Guinier, G. Fournet, *Small angle scattering of X-rays* (John Wiley & Sons Inc., New York, 1955).
25. G. Kostorz, in *Treatise on Materials Science and Technology*, edited by G. Kostorz (Academic Press, 1979), p. 227.
26. O. Glatter, O. Kratky, *Small-angle X-ray scattering* (Academic Press, London, 1982).
27. P.W. Schmidt, D. Avnir, D. Levy, A. Hoehr, M. Steiner, A. Roell, J. Chem. Phys. **94**, 1474 (1991).
28. M. Calvo-Dahlborg, J.M. Ruppert, in *Proceeding International Workshop on "Mechanical Properties of Metallic Glasses", Ústav experimentálnej fyziky SAV, Kosiče, Slovakia, 22–24 September 1998*, p. 9.
29. J.M. Ruppert, Diplôme d'Études Approfondies (DEA), École des Mines, Nancy, France, Sept. 1998.